

# DGAR: A Unified Domain Generalization Framework for RF-Enabled Human Activity Recognition

Junshuo Liu, *Graduate Student Member, IEEE*, Xin Shi, *Member, IEEE*, Robert C. Qiu, *Fellow, IEEE*

**Abstract**—Radio-frequency (RF)-based human activity recognition (HAR) is a non-intrusive and privacy-preserving technology with applications in smart homes, healthcare, and security systems. However, real-world deployments face challenges from domain shifts caused by user behavior, physical attributes, and environmental conditions, leading to performance degradation. To address this, we propose DGAR, a domain-generalized activity recognition framework that learns domain-invariant and domain-specific representations without requiring target domain data. DGAR leverages correlation alignment to reduce inter-domain discrepancies and integrates a squeeze-and-excitation (SE) block to enhance the extraction of salient spatial and temporal features from RF data. Extensive experiments on multiple public datasets, including HUST-HAR, Lab-LFM, and Office-LFM, validate DGAR’s effectiveness, achieving F1-score improvements ranging from 2.09% to 5.81% over state-of-the-art methods. These results demonstrate DGAR’s ability to address domain shift challenges, paving the way for robust, real-world HAR applications in diverse and dynamic scenarios.

**Index Terms**—Channel state information, domain generalization, human activity recognition, RF sensing.

## I. INTRODUCTION

HUMAN activity recognition (HAR) is a pivotal technology in human-computer interaction, focusing on identifying and interpreting human activities through data analysis. Among various methodologies, radio-frequency (RF)-based HAR has garnered substantial attention for its non-intrusive nature, adaptability to diverse environments, and inherent privacy-preserving characteristics [1]–[3]. RF-based HAR leverages wireless signals, such as Wi-Fi [4] and ultra-wideband (UWB) [5], to detect and classify activities by analyzing variations in signal propagation caused by human movements [6]. A key component of RF-based HAR is channel state information (CSI), which encodes detailed propagation characteristics between the transmitter and receiver, encompassing both amplitude and phase data [7], [8].

CSI’s high-resolution representation of the wireless channel allows the detection of subtle environmental changes, which is critical for accurate activity recognition [9], [10].

Manuscript received April xx, 202x; revised August xx, 202x. This work was supported in part by the Nation Natural Science Foundation of China under Grant No.12141107 and in part by the Interdisciplinary Research Program of HUST, 2023JCYJ012. (*Corresponding author: Xin Shi.*)

J. Liu, and R. Qiu are with the School of Electronic Information and Communications, Huazhong University of Science and Technology, Wuhan 430074, China (e-mail: junshuo\_liu@hust.edu.cn; aiming@hust.edu.cn).

X. Shi is with the Energy Internet Research Institute, Tsinghua University, Beijing 100085, China (e-mail: xinshi\_bjcy@163.com).

Its seamless integration into existing wireless infrastructures further underscores its suitability for applications such as smart homes, healthcare monitoring, fall detection for the elderly, and security systems [11]–[14].

Recent advancements in machine learning have significantly improved HAR performance. Traditional models, including support vector machines (SVM) [15] and random forests (RF) [16], rely on manually crafted features extracted from CSI data. However, their scalability and adaptability are often limited in dynamic environments. In response, deep learning architectures have emerged as a dominant paradigm, capable of automatically learning hierarchical features from raw CSI data. Noteworthy examples include convolutional neural networks (CNNs) [17], which excel at capturing spatial dependencies; long short-term memory networks (LSTMs) [18], adept at modeling temporal sequences; and Transformer-based models [19], leveraging attention mechanisms to capture long-range dependencies. These methodologies have been further advanced by hybrid architectures and innovative techniques [20], designed to bolster HAR systems’ efficacy, particularly in complex scenarios.

Despite these developments, model generalization remains a persistent challenge in RF-based HAR. HAR models often underperform when tested on unseen datasets, primarily due to the variability in RF signals caused by individual behaviors, physical characteristics, and environmental interactions [14], [21]. For instance, Fig. 1 illustrates the CSI distribution disparity between two users in the HUST-HAR dataset [22], captured using identical devices. This phenomenon, often expressed as  $P(\mathcal{D}_1) \neq P(\mathcal{D}_2)$ , exemplifies the domain shift issue, where a model trained on  $\mathcal{D}_1$  and  $\mathcal{D}_2$  performs poorly on a new subject ( $\mathcal{D}_{\text{test}}$ ) with a distinct distribution. This degradation is attributed to the non-independent and identically distributed (non-IID) nature of training and testing datasets, as corroborated by prior studies [23], [24].

To mitigate domain shift issue, transfer learning and domain adaptation methods have been extensively investigated [25], [26]. While transfer learning relies on pre-training a model on source domains and fine-tuning on target data, domain adaptation aligns source and target domain distributions through instance reweighting or feature transformation [27], [28]. However, both approaches require target domain data during training, which is often impractical for real-world applications, including personalized healthcare and fall detection. The difficulty of acquiring comprehensive target domain data underscores the need for solutions that align with a “train once,

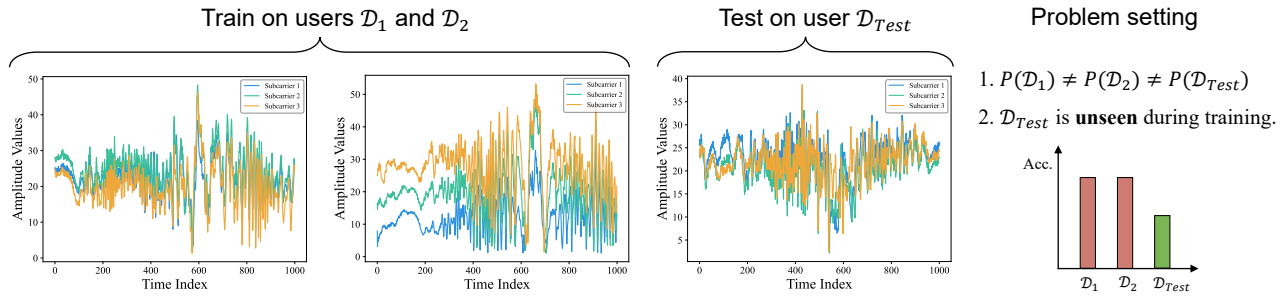


Fig. 1. Variation in CSI value distributions among different users. Existing HAR methods experience performance degradation when the test dataset exhibits a distinct distribution and remains inaccessible during training.

deploy everywhere” paradigm.

Domain generalization (DG) has emerged as a promising direction to address this limitation [29], [30]. Unlike transfer learning or domain adaptation, DG focuses on building models that generalize to unseen target domains without requiring target data during training [31]. Despite DG’s notable success in fields such as computer vision [32], [33], its application to RF-based HAR poses unique challenges, including the high dimensionality of RF data, its sensitivity to environmental variations, and the complex interplay between RF signals and human activities.

In this paper, we introduce domain-generalized activity recognition (DGAR), a framework designed to address domain shift in RF-based HAR. DGAR employs a unified deep neural network architecture that concurrently learns domain-invariant and domain-specific representations, leveraging their complementary strengths:

- Domain-invariant representation learning: This component extracts features shared across all training domains, minimizing inter-domain discrepancies and enabling improved transferability to unseen domains.
- Domain-specific representation learning: This component captures the unique characteristics of each training domain, preserving diversity in feature representations to mitigate overfitting and enhance generalization.

The integration of these components enables DGAR to effectively balance domain-specific and domain-invariant features, resulting in superior generalization capabilities. By incorporating advanced deep learning techniques tailored for high-dimensional RF data, DGAR ensures robust spatial and temporal feature extraction. Extensive experiments on publicly available HAR datasets validate DGAR’s effectiveness, demonstrating its potential to advance the state-of-the-art in RF-based HAR while addressing the critical challenge of domain generalization.

The main contributions of this paper are fourfold:

- We introduce DGAR, a unified domain generalization framework tailored for RF-enabled HAR, addressing the critical challenge of cross-person activity recognition. DGAR effectively mitigates the domain shift problem, achieving robust generalization to unseen individuals and environments.
- Our framework incorporates a domain-invariant representation learning module, employing correlation alignment

to minimize inter-domain discrepancies. By aligning feature distributions across domains and optimizing a robust distance metric, our approach enhances transferability and ensures strong generalization to unseen scenarios.

- To improve the extraction of meaningful features from RF data, we integrate a squeeze-and-excitation (SE) block into the architecture. The SE block recalibrates feature importance dynamically across RF subcarriers and antennas, significantly enhancing the capture of spatial and temporal dependencies and contributing to improved model generalization.
- We conduct extensive experiments across multiple RF sensing techniques and diverse indoor environments. Results consistently show that DGAR outperforms baseline methods across key benchmarks, underscoring its potential to advance the state-of-the-art in RF-based HAR.

This paper is organized as follows. Section II reviews background and related work. Section III describes the proposed DGAR. Extensive experimental evaluations are provided in Section IV, and Section V concludes the paper.

## II. BACKGROUND AND RELATED WORK

### A. RF Channel Modeling

RF sensing methods typically exploit CSI to distinguish human activities or gestures. In this subsection, we first model the RF channel, then discuss two commonly used RF signal types: Wi-Fi and linear frequency modulation (LFM).

According to [34], in an indoor multipath environment with  $P$  propagation paths, the baseband RF channel model for a transmitter-receiver pair at a carrier frequency  $f_c$  can be expressed as:

$$h(t) = \sum_{p=1}^P \alpha_p e^{-j2\pi f_c \tau_p} + n(t), \quad (1)$$

where  $\alpha_p$  is the amplitude of the  $p$ -th path, and  $n(t)$  is Gaussian noise. Additionally,  $\tau_p = \tau_p^S + \tau_p^D$ , where  $\tau_p^S$  and  $\tau_p^D$  denote time delays caused by static and dynamic reflections, respectively. For a transmitted signal  $s(t)$ , the received signal is  $y(t) = h(t) * s(t)$ , where  $*$  denotes convolution. For simplicity, subsequent derivations focus on a single propagation path (omitting the subscript  $p$ ) and ignore the noise term.

**Wi-Fi Radio.** Wi-Fi communication systems typically employ orthogonal frequency division multiplexing (OFDM) to

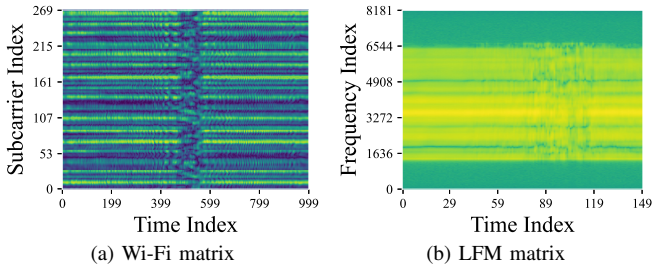


Fig. 2. Heatmaps for two RF techniques representing the "walking" activity.

distribute digital information across  $N$  distinct subcarriers. Let  $s_n$  denote the baseband transmitted signal on the  $n$ -th subcarrier. Under the narrowband assumption, where all subcarriers experience approximately the same delay  $\tau$ , the received signal for the  $n$ -th subcarrier is given by [34]:

$$y_n^W = \alpha_n e^{-j2\pi f_n \tau} s_n, \quad n \in \{1, \dots, N\}, \quad (2)$$

where  $\alpha_n$  and  $f_n$  denote the amplitude and frequency of the  $n$ -th subcarrier, respectively, and  $\tau$  represents the effective path delay. The complex channel state  $\hat{h}_n$  for each subcarrier can be estimated as  $\hat{h}_n = y_n^W / s_n$ .

When multiple OFDM packets are collected over time, the CSI estimates form a two-dimensional matrix of size  $N \times T$ , where  $N$  is the number of subcarriers and  $T$  is the number of sequentially received packets. This CSI matrix captures both amplitude and phase information over time, making it valuable for RF sensing applications such as activity recognition or motion detection. Fig. 2 (a) shows an example of a Wi-Fi matrix.

**LFM Radio.** LFM systems differ from OFDM by continuously sweeping over a bandwidth  $B$  within a predefined interval  $T_S$ , with a sweep rate  $\beta = B/T_S$ . The transmitted LFM signal can be written as:

$$x^L(t) = e^{j2\pi\left(f_c t + \frac{\beta t^2}{2}\right)}, \quad 0 \leq t \leq T_S, \quad (3)$$

where  $f_c$  is the starting frequency of the sweep. After propagating through the channel with a delay  $\tau$ , the received signal becomes:

$$y^L(t) = \alpha e^{-j2\pi\left(f_c(t-\tau) + \frac{\beta(t-\tau)^2}{2}\right)} \Pi(t-\tau), \quad (4)$$

where  $\alpha$  denotes the channel gain and  $\Pi(\cdot)$  is a rectangular window capturing the active chirp duration ( $0 \leq t - \tau \leq T_S$ ) [35]. In practice, the received signal is sampled and processed using fast Fourier transform (FFT)-based methods to extract frequency-domain features [36].

When  $T$  consecutive "snapshots" are collected, each snapshot is processed into  $N$  frequency bins (or chirp segments). These measurements form an  $N \times T$  matrix, reflecting the LFM channel's frequency and time variations, as shown in Fig. 2 (b).

Despite differences in how  $N$  and  $T$  are interpreted in OFDM (subcarrier indices and packets) versus LFM (frequency bins and snapshots), both methods yield rich 2D

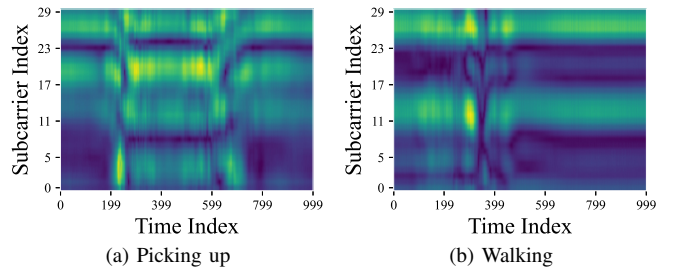


Fig. 3. Wi-Fi CSI heatmaps of two different activities: picking up and walking. Recognizing these activities intuitively is nearly impossible for human observers.

data structures. These matrices can be analyzed with signal-processing or learning-based methods to extract micro-motion features, recognize gestures, or perform activity recognition.

### B. RF Sensing Meets Machine Learning

Modern RF-based HAR research leverages fine-grained CSI to capture detailed spatiotemporal motion patterns. Commercial Wi-Fi devices, such as Intel 5300 Wi-Fi cards [37], and specialized RF systems [38] enable the extraction of CSI, offering richer insights into human activities compared to traditional methods. However, as illustrated in Fig. 3, discerning subtle differences—such as picking up an object versus walking—remains challenging for human observers due to the complexity and variability of CSI heatmaps.

To address this challenge, advanced machine learning (ML) and deep learning (DL) techniques automatically extract discriminative features from CSI data. These approaches effectively process both amplitude and phase information, thereby enabling robust HAR in complex environments. Traditional ML methods commonly rely on handcrafted features—such as statistical metrics, wavelet transforms, or Doppler signatures [39], [40]—derived from domain expertise. In contrast, DL models, including CNNs, recurrent neural networks (RNNs), and Transformers, learn hierarchical spatiotemporal features from raw or minimally preprocessed RF data [17]–[19], [41]. This shift reduces the need for extensive feature engineering while improving recognition accuracy.

Despite these advancements, most conventional approaches assume that training and testing data share the same underlying distribution. Such an independent and identically distributed assumption frequently leads to performance degradation when models are deployed in new, unseen scenarios characterized by diverse environments, user populations, and deployment conditions.

### C. Transfer Learning and Domain Adaptation

Domain shift is a significant challenge in RF-based HAR. Such shifts arise from factors including user populations (e.g., age, height, gait), indoor settings (e.g., room dimensions, furniture, building materials), hardware configurations (e.g., antenna arrays, sampling rates, operating frequencies), and deployment setups (e.g., angles, distances, occlusions). Models trained on a single source domain often exhibit degraded

performance when tested on novel target domains. To tackle this problem, transfer learning and domain adaptation (DA) have emerged as essential techniques.

Transfer learning leverages a model pre-trained on a source domain and fine-tunes it on a target domain with limited labeled data, thus reducing the need for retraining from scratch. Advanced strategies—such as teacher-student frameworks, self-distillation, and few-shot learning—enhance cross-domain performance. For instance, Thukral *et al.* [42] proposed a few-shot transfer learning framework that uses limited labeled target-domain data combined with self-supervised learning and data augmentation to mitigate domain gaps. Similarly, Zhao *et al.* [43] constructed a large-scale correlated dataset by merging multiple domains and categorizing activities into basic and complex groups, thus facilitating the learning of universal features during pre-training and improving model generalization across diverse domains.

Domain adaptation, in contrast, extends transfer learning by handling unlabeled or sparsely labeled target-domain data. DA techniques—including adversarial learning and distribution alignment—aim to minimize domain discrepancies between source and target data. Zhou *et al.* [44] introduced XHAR, a DA framework that pairs CNNs and Bidirectional Gated Recurrent Units (BiGRU) for spatiotemporal feature extraction with multiple domain discriminators to align distributions across devices and users. Chen *et al.* [45] developed Dynamic Associate Domain Adaptation (DADA), a semi-supervised Wi-Fi-based HAR framework that incorporates an attention-based DenseNet model and dynamically balances labeled and unlabeled target data, thereby achieving robust recognition in dynamic environments.

Nevertheless, both transfer learning and DA require some target-domain data during training. In many real-world HAR applications, this requirement is impractical because target tasks are often novel and remain inaccessible during training. Consequently, models must possess strong generalization capabilities to perform effectively in unseen domains. This constraint highlights the significance of domain generalization, which addresses the scenario where the target domain is entirely unknown during training.

#### D. Domain Generalization

Domain Generalization is an emerging research area that aims to build models capable of generalizing to unseen target domains by leveraging multiple source domains [29]. Unlike domain adaptation, which assumes some target data is available during training, DG operates under the assumption that the target domain is entirely unknown in the training phase. This distinctive setting makes DG particularly valuable for real-world HAR tasks, where models must handle novel and heterogeneous environments, users, and deployment scenarios.

A primary challenge in DG is to learn a prediction function that remains robust across unknown domains. Recent studies have proposed diverse strategies to enhance feature invariance and inter-domain alignment. For instance, Qin *et al.* [30] introduced Adaptive Feature Fusion for Activity Recognition (AFFAR), a DG framework that dynamically fuses domain-invariant and domain-specific features, thereby improving

generalization performance on public HAR datasets. Yao *et al.* [46] designed a DG framework for unobtrusive fall detection using radar signals, employing domain-specific subclassifiers, entropy regularization, and radar-specific data augmentations to achieve robust generalization across unseen environments and user populations. Similarly, Liu *et al.* [47] proposed DGSSL, a semi-supervised DG framework for people-centric activity recognition that integrates semi-supervised learning, adversarial training, and reconstruction tasks, resulting in superior domain alignment and task consistency on multiple real-world sensing datasets. These advancements underscore the critical role of DG in HAR, particularly for handling dynamic, unpredictable real-world conditions.

Notably, RF signals exhibit complex propagation effects and noise patterns that differ substantially from those in other sensor modalities, presenting unique challenges when applying DG techniques. While our method builds upon principles similar to AFFAR’s adaptive feature fusion, it is specifically tailored to capture the distinctive spatiotemporal signatures of RF signals under domain shifts. By simultaneously learning domain-specific and domain-invariant representations, without relying on any target-domain data, our framework aims to deliver robust performance in previously unseen RF environments.

### III. PROPOSED METHOD

In this section, we present a comprehensive overview of our proposed framework for domain-generalized activity recognition. First, we define the problem setting and outline the primary challenges. Next, we describe the main components of our approach, including the feature extraction pipeline, domain-specific modules, and the domain-invariant learning module. Finally, we discuss how these components are integrated into a unified training and inference procedure.

#### A. Problem Definition: Domain-Generalized Activity Recognition

Consider a standard HAR problem, where the training set  $\mathcal{D}_{\text{train}} = \{(\mathbf{x}_i, y_i)\}_{i=1}^n$  contains  $n$  instances. Each instance  $\mathbf{x} \in \mathbb{R}^d$  represents a  $d$ -dimensional sample, and  $y \in \{1, 2, \dots, C\}$  denotes the corresponding activity category (e.g., walking, sitting). The goal is to learn a model  $f : \mathbf{x} \rightarrow y$  that accurately classifies activities within the training set, i.e., to find:

$$f^* = \arg \min_f \frac{1}{n} \sum_{i=1}^n \ell(f(\mathbf{x}_i), y_i), \quad (5)$$

where  $f^*$  is the optimal model and  $\ell(\cdot)$  is a suitable loss function, such as the cross-entropy loss.

However, minimizing the training error does not guarantee strong performance on unseen test data  $\mathcal{D}_{\text{test}}$ . For example, a well-trained HAR model may fail to generalize to individuals with different body shapes or movement patterns, especially if these domain-specific characteristics are absent from the training set. Moreover, it is infeasible to collect training samples that cover all potential real-world variations, making it challenging to develop a truly generalized model.

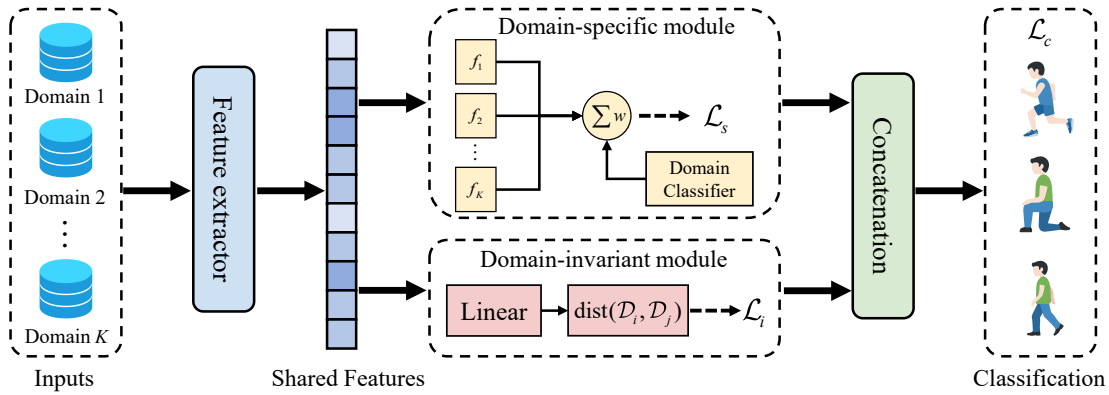


Fig. 4. Illustration of the DGAR framework.

Although meta-learning, transfer learning, and domain adaptation [42], [48], [49] have been investigated in cross-domain scenarios, these methods typically assume access to the target domain during training. This assumption does not hold in many practical applications, where the target domain remains entirely unknown at training time.

To address this issue, we focus on domain-generalized activity recognition, where each "domain" broadly corresponds broadly to a "dataset" or a partition thereof [29]. Specifically, we assume access to  $K$  distinct but related training domains,  $\mathcal{D}_{\text{train}} = \{\mathcal{D}_1, \mathcal{D}_2, \dots, \mathcal{D}_K\}$ , with each domain  $\mathcal{D}_k = \{(\mathbf{x}_i^k, y_i^k)\}_{i=1}^{n_k}$  containing  $n_k$  samples. Our objective is to learn a domain-generalized model  $f$  that, once trained on these  $K$  source domains, can achieve minimum error on an unseen target domain  $\mathcal{D}_{\text{test}} = \{(\mathbf{x}_i, y_i)\}_{i=1}^{n_{\text{test}}}$ .

All domains share the same feature space and label space, i.e.,  $\mathcal{X}_{\text{train}} = \mathcal{X}_{\text{test}}$  and  $\mathcal{Y}_{\text{train}} = \mathcal{Y}_{\text{test}}$ . In practice, however, the underlying data distributions vary across domains, such that

$$P_i(\mathbf{x}) \neq P_j(\mathbf{x}) \neq P_{\text{test}}(\mathbf{x}), \quad 1 \leq i \leq j \leq K. \quad (6)$$

These domain shifts make domain-generalized activity recognition a suitable benchmark for evaluating the robustness and generalizability of HAR methods.

## B. Main Idea

In this paper, we propose DGAR, a novel approach designed under the realistic constraint that test data are inaccessible during training. Despite this limitation, we assume that test samples can be approximated by aggregating existing training data. This assumption is supported by the observation that although individuals may generate distinct CSI signals while performing the same activity, their body shapes and activity styles often share commonalities. Consequently, we represent an unseen test sample as a weighted combination of domain-specific features extracted from the known training domains. Simultaneously, to mitigate inter-domain discrepancies and facilitate knowledge transfer, we also enforce the learning of domain-invariant features.

The core of DGAR, therefore, lies in learning both domain-specific and domain-invariant representations. Domain-specific

representation learning captures the unique characteristics of each source domain, thereby improving flexibility to accommodate diverse data distributions. In contrast, domain-invariant representation learning aims to extract features that generalize across domains and thus remain applicable to unseen data. Fig. 4 illustrates the DGAR framework.

Conceptually, DGAR comprises four modules: (1) a feature extraction module that processes raw CSI data with shared parameters to control model size and computational cost; (2) a domain-specific representation learning module that attaches  $M$  fully connected (FC) layers for each domain to encode domain-specific attributes; (3) a domain-invariant module that uses a distribution alignment loss to reduce inter-domain discrepancies; (4) an activity classification module that fuses these representations to predict the activity label.

As summarized in Table I, the feature extraction module includes two residual blocks with 1D convolutions, two max-pooling layers for temporal downsampling, an SE block for channel attention, and a global average pooling layer. Each domain-specific branch then adds  $M$  FC layers to the extracted features, capturing distinctive attributes of each domain. A weighting function adaptively aggregates these specialized representations to approximate the unseen target domain's representation. Meanwhile, a distribution alignment loss in the domain-invariant module encourages robust, generalizable features. Finally, an FC-based activity classification module uses these fused features to generate the final activity prediction.

Formally, DGAR is trained using a multi-term objective function that integrates classification, domain-specific representation, and domain-invariant representation losses:

$$\mathcal{L} = \mathcal{L}_c + \lambda \mathcal{L}_s + \gamma \mathcal{L}_i, \quad (7)$$

where  $\lambda$  and  $\gamma$  are tradeoff hyperparameters. The classification loss

$$\mathcal{L}_c = -\frac{1}{M} \sum_{i=1}^M y_i \log P(y_i | x_i), \quad (8)$$

is the cross entropy loss, and  $M = \sum_{k=1}^K n_k$  is the total number of training samples. The following subsections detail how

<sup>1</sup>Each convolutional layer in the residual blocks is followed by a batch normalization (BN) layer and a ReLU activation.

TABLE I  
FEATURE EXTRACTION MODULE ARCHITECTURE<sup>1</sup>

Layer	Input Shape	Output Shape
<i>Residual Block 1</i>		
Conv1	$B \times D \times L$	$B \times 128 \times L$
Conv2	$B \times 128 \times L$	$B \times 128 \times L$
Shortcut	$B \times D \times L$	$B \times 128 \times L$
<b>MaxPool</b>	$B \times 128 \times L$	$B \times 128 \times L/2$
<i>Residual Block 2</i>		
Conv1	$B \times 128 \times L/2$	$B \times 256 \times L/2$
Conv2	$B \times 256 \times L/2$	$B \times 256 \times L/2$
Shortcut	$B \times 128 \times L/2$	$B \times 256 \times L/2$
<b>MaxPool</b>	$B \times 256 \times L/2$	$B \times 256 \times L/4$
<b>SE Block</b>	$B \times 256 \times L/4$	$B \times 256 \times L/4$
<b>Global AvgPool</b>	$B \times 256 \times L/4$	$B \times 256$

the domain-specific and domain-invariant modules collectively enhance domain generalization.

### C. Domain-Specific Representation Learning

The domain-specific representation learning module specializes the model to each training domain while allowing these specialized components to be fused for the unseen target. Mathematically, for a new test sample  $\mathbf{x}$ , its feature vector  $\mathbf{z}$  is an aggregation of domain-specific features:

$$\mathbf{z} = \sum_{k=1}^K w_k f_k(f_e(\mathbf{x})), \quad \text{where } w_k > 0 \text{ and } \sum_{k=1}^K w_k = 1, \quad (9)$$

where  $w_k$  indicates the relevance of domain  $\mathcal{D}_k$ ,  $f_k$  denotes the domain-specific layers for  $\mathcal{D}_k$ , and  $f_e$  is the shared feature extractor.

This strategy can be viewed as a form of ensemble learning, where each domain-specific branch acts as a base learner. The shared CNN feature extractor  $f_e$  provides general representations, while the higher layers  $f_k$  adapt to domain-specific variations [50].

To determine  $w_k$  dynamically, we employ a domain classifier  $f_d : \mathbf{x} \rightarrow \mathbb{R}^K$ , which predicts the likelihood that  $\mathbf{x}$  belongs to each source domain based on the shared CNN features. We then apply a softmax function to obtain valid weights  $(w_1, \dots, w_K)$ . During training, the true domain label  $d_k$  of each sample is known (i.e.,  $d_k = k$ ), enabling a domain-specific loss:

$$\mathcal{L}_s^k = \frac{1}{n_k} \sum_{i=1}^{n_k} \ell(f_d(f_e(\mathbf{x}_i)), d_k), \quad (10)$$

where  $n_k$  is the number of samples in domain  $\mathcal{D}_k$ . The total domain-specific loss is

$$\mathcal{L}_s = \frac{1}{K} \sum_{k=1}^K \mathcal{L}_s^k. \quad (11)$$

During inference on the target domain, the network applies the domain classifier’s output as weights for each source branch to fuse the domain-specific features. Because the target

domain is unknown, these learned weights act as a proxy for domain similarity, allowing DGAR to adaptively combine relevant characteristics from the source domains without having observed target-domain data in advance.

### D. Domain-Invariant Representation Learning

While domain-specific representation learning is crucial for capturing specialized information, it can also exacerbate feature distribution gaps. To promote generalization, we introduce a domain-invariant representation learning module that reduces the distribution mismatch among source domains.

Since lower layers in deep networks often learn domain-agnostic features and higher layers capture domain-specific cues [50], we incorporate a feature adaptation mechanism in the higher layers. Under domain generalization, the target domain is unavailable during training, so we instead align distributions among all  $K$  source domains  $\{\mathcal{D}_1, \dots, \mathcal{D}_K\}$ .

Specifically, we adopt correlation alignment (CORAL) [51] to align second-order statistics across domains. Let  $\mathbf{z}_i$  be features from domain  $\mathcal{D}_i$ , and let  $\Sigma_i$  be the corresponding sample covariance matrix. The distance between two domains  $\mathcal{D}_i$  and  $\mathcal{D}_j$  is:

$$\text{dist}(\mathcal{D}_i, \mathcal{D}_j) = \|\Sigma_i - \Sigma_j\|_F^2. \quad (12)$$

To ensure domain invariance among all  $K$  source domain, we sum (or average) this pairwise distance:

$$\mathcal{L}_i = \frac{2}{K(K-1)} \sum_{1 \leq i < j \leq K} \|\Sigma_i - \Sigma_j\|_F^2, \quad (13)$$

where  $\|\cdot\|_F$  denotes the Frobenius norm. By minimizing  $\mathcal{L}_i$ , the source-domain feature distributions become more similar, thereby producing representations that are more robust to unseen target domains.

### E. Training and Inference

Algorithm 1 outlines the overall DGAR training process, from parameter initialization through iterative optimization.

During training, we sample mini-batches from each of the  $K$  source domains and pass them through the shared feature extractor  $f_e$ . The resulting lower-level features are fed into each domain-specific branch  $f_k$  to learn high-level, domain-specific representations, and into a domain classifier  $f_d$  that produces softmax-based weights for fusing these representations. Simultaneously, a distribution alignment loss is computed among the source domains to encourage domain invariance. The fused features are then passed to an activity classifier, and the entire model—including the domain-specific, domain-invariant, and classifier modules—is updated by minimizing the overall loss.

During inference, the learned parameters remain fixed. Each unseen target sample goes through the same feature extractor to obtain lower-level representations, which are then passed to the domain classifier. The classifier’s softmax output provides weights  $(w_1, \dots, w_K)$ , indicating how similar the sample is to each source domain. These weights adaptively combine the domain-specific features from the  $K$  branches, creating a robust, fused representation for activity classification on the unseen domain.

**Algorithm 1:** Overall learning procedure of DGAR.

---

**Input** :  $K$  training domains  $\mathcal{D}_1, \dots, \mathcal{D}_K$ , and hyperparameters  $\lambda, \gamma$ .

**Output:** Classification results on the unseen test domain.

- 1 **Initialize** the model parameters  $\theta$  randomly;
- 2 **while** *not converged* **do**
- 3     Sample a mini-batch  $\mathcal{B} = \{\mathcal{B}_1, \dots, \mathcal{B}_K\}$  from the  $K$  domains;
- 4     Extract the lower-level features  $f_e(\mathbf{x})$  using the feature extractor;
- 5     Extract the domain-specific features  $f_k(f_e(\mathbf{x}))$  via the  $K$  domain-specific branches;
- 6     Compute the domain-specific loss  $\mathcal{L}_s$  and obtain the weight for each source branch;
- 7     Compute the domain-invariant loss  $\mathcal{L}_i$ ;
- 8     Fuse the domain-specific features with weights according to (9);
- 9     Calculate the total loss  $\mathcal{L}$ ;
- 10    Update the model parameters  $\theta$  using Adam.
- 11 **end**
- 12 Make inference on the target HAR data.

---

## IV. EXPERIMENTAL EVALUATION

This section presents a comprehensive evaluation of the proposed DGAR approach in the context of domain-generalized activity recognition.

## A. Datasets and Preprocessing

We employ three RF-based activity datasets, each partitioned into distinct domains as follows.

**HUST-HAR.** The HUST-HAR dataset [22] was collected using two PCs equipped with Intel 5300 Wi-Fi cards as both transmitters and receivers. It consists of six human activities—lying down, picking up, sitting down, standing, standing up, and walking—performed by six subjects. Each subject repeated each activity 100 times, yielding 600 samples per activity. To simulate the domain-generalized HAR scenario, we divided the six subjects into three groups of two subjects each; data from each group formed one domain, resulting in three domains in total.

**Lab-LFM.** The Lab-LFM dataset was acquired in a laboratory environment using a USRP-based system. One horn antenna transmitted an LFM signal, while another horn antenna receives it; a PC controlled the USRP device, handling signal acquisition and processing. Six individuals (one female and five males, aged 20 to 30) performed six activities—kicking, picking up, sitting down, standing, standing up, and walking—each repeated 50 times, for a total of 300 samples per activity (1,800 samples overall). We formed three domains by grouping these individuals into three pairs. In addition, a transmissive reconfigurable intelligent surface was employed to enable through-wall HAR.

**Office-LFM.** Similar to Lab-LFM, the Office-LFM dataset was collected using a USRP-based LFM system, but in an

office environment. Ten participants (three females and seven males, aged 20 to 30) performed the same six activities, each repeated 50 times, totaling 3,000 samples. We created five domains by grouping the ten participants into five pairs.<sup>2</sup>

In each experiment, one domain serves as the test domain, and the remaining domains are used for training. We also reserve 20% of the training data as a validation set for hyperparameter tuning. Our primary goal is to investigate cross-person scenarios within each dataset, where different individuals share the same transmitter-receiver setup.

## B. Comparison Methods and Implementation Details

We compare DGAR against several state-of-the-art DG methods:

- **Empirical Risk Minimization (ERM)** [52]: Minimizes the average error across all training data. ERM serves as a naive baseline by training a single model on all source domains without addressing domain shifts.
- **Invariant Risk Minimization (IRM)** [53]: Promotes the extraction of features invariant across different domains, thus enhancing generalization to unseen domains.
- **Domain-Adversarial Neural Network (DANN)** [27]: Uses an adversarial network composed of a feature generator and a domain discriminator. The generator aims to produce domain-invariant features by misleading the discriminator, thus aligning feature distributions among the source domains.
- **Group Distributionally Robust Optimization (Group-DRO)** [54]: Focuses on minimizing the worst-group loss across predefined groups and employs additional regularization to emphasize the most challenging subsets of data.
- **Maximum Mean Discrepancy (MMD)** [55]: Measures the distance between domain distributions in a reproducing kernel Hilbert space and minimizes this distance to obtain domain-invariant representations.

We also include a baseline that directly trains on the target domain to represent the ideal scenario in which target-domain data are available for training:

- **ERM-T:** Trains a model on the target domain via ERM, splitting the target data into training and testing sets with a ratio of 8:2.

To evaluate DGAR’s classification performance under the domain generalization setting, we employ non-IID cross-person HAR tasks. Specifically, we partition the subjects into multiple groups; each group’s data constitute one domain. In each run, one domain is designated as the unseen target domain, and the remaining domains serve as source domains. We then train all models on the source domains and test them on the target domain. Hyperparameters are tuned using the validation set, and all models are trained under the same conditions to ensure a fair comparison.

We implement all models in PyTorch 2.2.2, maintaining a uniform neural network architecture. For optimization, we use

<sup>2</sup>Both the Lab-LFM and Office-LFM datasets are publicly available at [https://github.com/Junshuo-Lau/HUST\\_HAR\\_LFM](https://github.com/Junshuo-Lau/HUST_HAR_LFM).

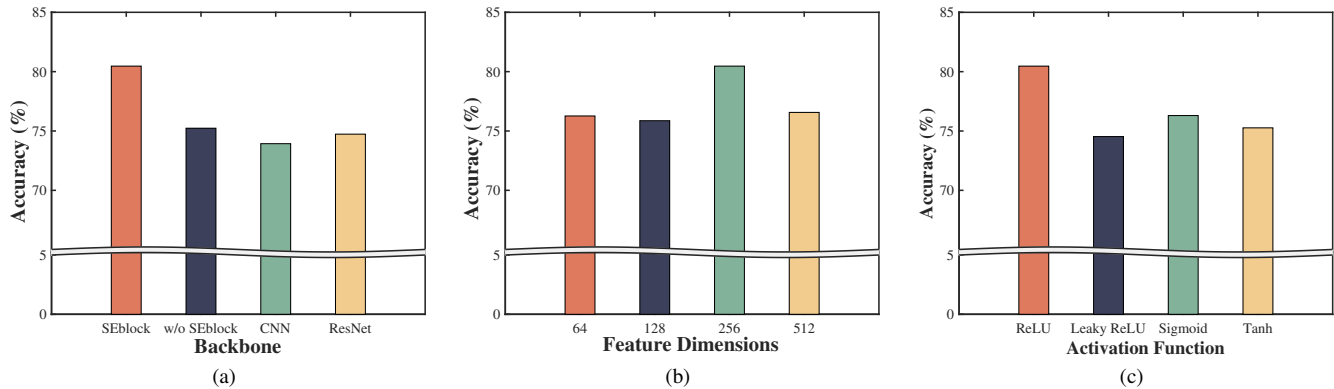


Fig. 5. Model parameter exploration of DGAR. (a) Impact of different backbones. (b) Influence of hidden dimension sizes. (c) Comparison of activation functions.

the Adam optimizer with an initial learning rate of  $10^{-4}$  for model parameters and  $10^{-3}$  for hyperparameters ( $\lambda$  and  $\gamma$ ). We apply weight decay of  $10^{-5}$  to reduce overfitting. Each batch consists of 32 samples, and training continues for up to 100 epochs. We employ early stopping based on validation performance and use a ReduceLROnPlateau scheduler, reducing the learning rate by 50% if the validation loss fails to improve for 10 consecutive epochs. All experiments are conducted on an NVIDIA RTX 3090 GPU.

We measure performance using the following metrics: (1) Accuracy, the proportion of correctly classified samples in the test domain; (2) Precision, the weighted average precision across classes; (3) Recall, the weighted average recall across classes; and (4) F1-score, the weighted average F1-score across classes that balances precision and recall.

### C. Model Parameter Exploration

We conduct extensive experiments on the Office-LFM datasets to identify optimal model parameters before proceeding with a fair comparison against other methods. Specifically, we investigate three critical aspects of our framework: backbone network selection, feature dimension size, and activation function selection.

1) *Backbone selection*: In order to capture rich and discriminative representations, we first study the impact of different backbones. We compare CNN, ResNet, the proposed method without (w/o) the SE block, and the proposed method with SE block. The results, shown in Fig. 5 (a), indicate that incorporating SE blocks consistently yields higher accuracy than the alternatives. We attribute this improvement to the enhanced channel-wise feature recalibration afforded by SE blocks, which effectively highlights more informative features and suppresses less useful ones. Based on these findings, we adopt the SE-block backbone as the default setting in subsequent experiments.

2) *Feature dimension size and activation function selection*: Next, we explore the dimensionality of the extracted features, defined by the output of a global average pooling layer. Specifically, the tensor of shape  $B \times 256 \times \frac{L}{4}$  is reduced to  $B \times 256$  after global average pooling. We then evaluate hidden feature dimensions  $\{64, 128, 256, 512\}$  to balance

representational capacity with computational overhead. As illustrated in Fig. 5 (b), a hidden dimension of 256 achieves the highest overall accuracy, reflecting its superiority in capturing discriminative information while remaining computationally feasible.

Finally, we compare several widely used activation function, including ReLU, Leaky ReLU, Sigmoid, and Tanh, as shown in Fig. 5 (c). Empirically, ReLU consistently outperforms the other candidates, suggesting that its non-saturating property facilitates more robust feature learning. Hence, we adopt ReLU throughout our framework.

### D. Classification Performance

Tables II, III, and IV demonstrate that DGAR achieves the highest weighted F1-scores on HUST-HAR, Lab-LFM, and Office-LFM, surpassing the second-best methods by 2.09%, 4.52%, and 5.81%, respectively. These results highlight the critical importance of integrating both domain-invariant and domain-specific information for effective cross-domain HAR. While DANN emphasizes learning domain-invariant representations through adversarial training, it does not match DGAR’s performance due to insufficient modeling of domain-specific characteristics. These characteristics are vital for capturing domain-specific nuances that enhance cross-domain generalization. Similarly, methods such as IRM and GroupDRO, which focus on invariant features and worst-case domain performance, respectively, fail to achieve consistent results comparable to DGAR. This underscores the effectiveness of a balanced approach that incorporates both invariant and domain-specific information for robust activity recognition across diverse domains.

When target domain data is included during training (ERM-T), the model surpasses all domain generalization methods, including DGAR. This result emphasizes the substantial benefit of access to target-specific data, enabling the model to fine-tune its representations to the target domain. However, in real-world scenarios, access to target domain data is often restricted, making robust domain generalization methods, such as DGAR, indispensable.

Another notable finding is that the average F1-scores on Office-LFM, which includes five sub-domains, are higher than



TABLE II  
WEIGHTED F1-SCORE (%) ON HUST-HAR DATASET.

Target	ERM	IRM	DANN	GroupDRO	MMD	DGAR (ours)	ERM-T
T-1	69.54	62.96	<u>69.56</u>	68.33	66.07	<b>71.30</b>	98.34
T-2	71.17	69.54	<u>71.69</u>	69.65	71.02	<b>74.86</b>	98.47
T-3	<u>61.60</u>	57.19	<u>57.86</u>	57.27	59.88	<b>62.43</b>	97.37
Average	<u>67.44</u>	63.23	66.37	65.08	65.66	<b>69.53</b>	98.06

The **bold** entry indicates the best result except for the ideal condition; the underlined entry indicates the second best.

TABLE III  
WEIGHTED F1-SCORE (%) ON LAB-LFM DATASET.

Target	ERM	IRM	DANN	GroupDRO	MMD	DGAR (ours)	ERM-T
T-1	66.92	67.30	69.90	70.00	<u>70.55</u>	<b>76.09</b>	98.61
T-2	64.20	63.39	60.79	65.91	<u>67.98</u>	<b>72.96</b>	97.50
T-3	61.13	59.76	58.77	61.46	<u>62.94</u>	<b>66.00</b>	96.38
Average	64.08	63.48	63.15	65.79	<u>67.16</u>	<b>71.68</b>	97.50

The **bold** entry indicates the best result except for the ideal condition; the underlined entry indicates the second best.

TABLE IV  
WEIGHTED F1-SCORE (%) ON OFFICE-LFM DATASET.

Target	ERM	IRM	DANN	GroupDRO	MMD	DGAR (ours)	ERM-T
T-1	62.22	66.64	64.22	69.00	<u>75.49</u>	<b>78.65</b>	99.17
T-2	67.83	66.39	64.35	68.22	<u>71.38</u>	<b>81.72</b>	98.34
T-3	69.69	70.71	69.04	72.19	<u>79.48</u>	<b>83.51</b>	100.00
T-4	66.82	66.87	65.29	68.17	<u>76.59</u>	<b>78.88</b>	98.33
T-5	61.32	65.51	55.53	65.18	<u>69.06</u>	<b>78.31</b>	95.84
Average	65.58	67.22	63.69	68.55	<u>74.40</u>	<b>80.21</b>	98.34

The **bold** entry indicates the best result except for the ideal condition; the underlined entry indicates the second best.

those on datasets with only three domains (HUST-HAR and Lab-LFM). This improvement is attributed to the increased diversity provided by the additional source domains, which helps the model learn more generalized and robust features. Greater domain diversity allows DGAR to balance the extraction of invariant features with domain-specific nuances, mitigating overfitting to a single domain and enhancing its ability to recognize activities under varied conditions.

In conclusion, the experimental results confirm that increasing the number of training domains improves data diversity and strengthens generalization. DGAR’s ability to integrate domain-invariant and domain-specific information enables superior cross-domain HAR performance, outperforming existing methods that focus exclusively on invariant features or fail to adequately model domain-specific information. These findings underscore the importance of a comprehensive feature representation approach for achieving robust and accurate activity recognition across diverse and unseen domains.

### E. Ablation Study

1) *Domain-invariant and domain-specific learning modules*: DGAR integrates two key components: a domain-invariant learning module and a domain-specific learning module. To assess the importance of each module, we perform an ablation study of four variants of our method: (1)  $\mathcal{L}_c$ , (2)  $\mathcal{L}_c + \mathcal{L}_i$ , (3)  $\mathcal{L}_c + \mathcal{L}_s$ , and (4) the complete DGAR framework. Fig. 6 (a) presents the classification accuracy of these variants

on different tasks, showing that the joint incorporation of both modules yields the strongest performance. These results underline the complementary roles of the domain-invariant and domain-specific modules in improving HAR accuracy.

2) *Extending domain-invariant learning with other distance*: To further validate DGAR’s flexibility, we replace CORAL loss with several alternative distribution-matching techniques, including MMD, Central Moment Discrepancy (CMD), and Sliced Wasserstein Discrepancy (SWD). As illustrated in Fig. 6 (b), DGAR maintains robust performance across different datasets regardless of the specific distance metric used. Although CORAL shows slightly better results in some scenarios, other methods, such as CMD and MMD, also exhibit strong performance. This underscores DGAR’s adaptability and robustness, affirming that it can seamlessly integrate diverse distribution alignment strategies to address various domain-adaptation challenges.

### F. Hyperparameter Tuning and Inference Efficiency

To evaluate the robustness of DGAR with respect to its hyperparameters, we conduct a sensitivity analysis on the Office-LFM dataset, which covers more domains than the other datasets. Specifically, we vary  $\lambda$  (domain-specific learning weight) and  $\gamma$  (domain-invariant learning weight) and measure the resulting accuracy (%).

As illustrated in Fig. 7, when either  $\lambda$  or  $\gamma$  is set too high or too low, there is a noticeable drop in model performance,

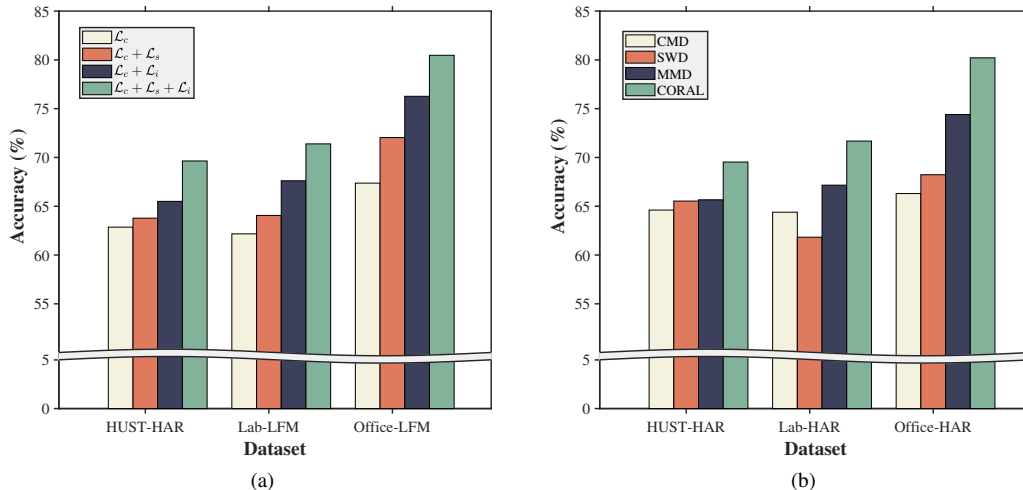


Fig. 6. Ablation studies of DGAR. (a) Effectiveness of domain-specific and domain-invariant learning modules. (b) Replacing CORAL loss with alternative distance metrics.

TABLE V  
COMPARISON OF INFERENCE EFFICIENCY AND ACCURACY ON THE OFFICE-LFM DATASET.

Target	ERM	IRM	DANN	GroupDRO	MMD	DGAR (ours)
Average elapsed time over 5 runs (s/run)	0.036	0.036	0.029	0.028	0.036	0.035
Throughput (samples/s)	16793.36	16744.80	20795.66	21284.65	16872.83	16977.73
Accuracy (%)	65.90	67.27	64.40	69.23	74.83	80.47

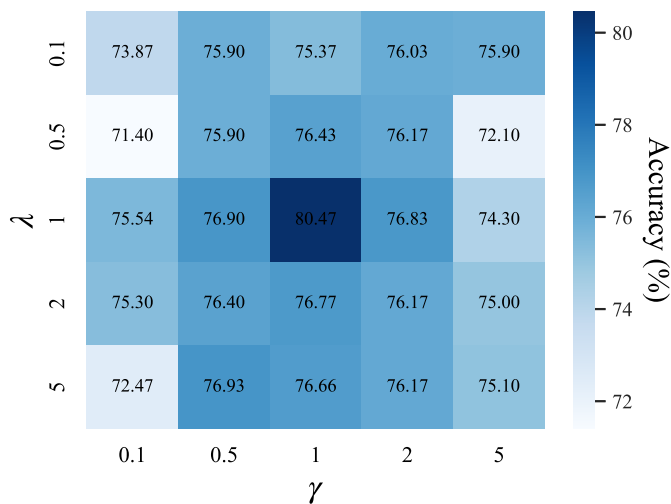


Fig. 7. Parameter Sensitivity Heatmap.

underscoring the necessity of balancing these two objectives. The best performance is achieved at  $\lambda = 1$  and  $\gamma = 1$ , yielding a accuracy of 80.47%. Nevertheless, other parameter settings, such as  $\lambda = 5, \gamma = 0.5$  and  $\lambda = 0.1, \gamma = 2$ , also produce competitive results. These observations suggest that DGAR displays a certain level of resilience across a range of hyperparameter settings, which is highly beneficial for real-world applications where extensive fine-tuning can be resource-intensive.

Table V compares the inference efficiency and the final classification accuracy for various baselines and our DGAR

method on the Office-LFM dataset. The inference speed is assessed based on two metrics: (1) the average elapsed time per inference run, computed over five consecutive runs on the entire test set; and (2) the throughput (i.e., samples per second), which indicates how many data samples can be processed in one second. Accuracy (%) is included to highlight the trade-off between computational efficiency and predictive performance.

From the table, although DANN and GroupDRO exhibit slightly faster inference speeds (higher throughput and shorter elapsed time), their accuracy remains below 70%. In contrast, DGAR achieves a competitive inference time of 0.035 s/run (processing 16,977.73 samples/s) while substantially improving the final accuracy to 80.47%. This observation suggests that DGAR not only maintains a near real-time classification rate but also provides superior recognition capabilities. Consequently, it stands out as a more balanced and robust solution for real-world activity recognition tasks, where both speed and accuracy are critical.

## V. CONCLUSION

In this paper, we introduced DGAR, a domain-generalized activity recognition framework tailored for RF-enabled human activity recognition. DGAR addresses the critical challenge of domain shifts by concurrently learning domain-invariant and domain-specific representations without requiring access to target domain data during training. This framework integrates correlation alignment to minimize inter-domain discrepancies and a squeeze-and-excitation block to dynamically enhance spatial and temporal feature extraction, ensuring robust and

efficient performance across diverse environments. Extensive experiments on three public datasets—HUST-HAR, Lab-LFM, and Office-LFM—demonstrated the superior generalization capability of DGAR. The framework consistently outperformed state-of-the-art methods, achieving notable improvements in F1-score, and exhibited strong adaptability to cross-person scenarios. These results underline DGAR’s potential to serve as a reliable solution for real-world HAR applications.

Future work will explore the integration of advanced techniques such as meta-learning and multimodal fusion to further enhance generalization capabilities. Additionally, extending DGAR to outdoor environments and incorporating lightweight architectures for real-time processing on edge devices will be investigated to broaden its applicability and efficiency in dynamic, real-world settings.

## APPENDIX A

### ADDITIONAL DISTRIBUTION ALIGNMENT TECHNIQUES

In addition to CORAL [51], various other distribution alignment methods have been extensively studied. This section provides a concise overview of three notable approaches: Maximum Mean Discrepancy (MMD) [55], Central Moment Discrepancy (CMD) [56], and Sliced Wasserstein Distance (SWD) [57]. These techniques can function as either alternatives or complements to CORAL for mitigating domain shifts in domain-generalized activity recognition.

#### A. Maximum Mean Discrepancy (MMD)

MMD evaluates the distance between two distributions by embedding them in a reproducing kernel Hilbert space (RKHS). Let  $\{\mathbf{x}_i\}_{i=1}^m$  and  $\{\mathbf{y}_j\}_{j=1}^n$  be samples from distributions  $P$  and  $Q$ , respectively. The squared MMD is commonly expressed as:

$$\begin{aligned} \text{MMD}^2(P, Q) &= \frac{1}{m^2} \sum_{i=1}^m \sum_{j=1}^m \mathcal{K}(\mathbf{x}_i, \mathbf{x}_j) \\ &+ \frac{1}{n^2} \sum_{i=1}^n \sum_{j=1}^n \mathcal{K}(\mathbf{y}_i, \mathbf{y}_j) - \frac{2}{mn} \sum_{i=1}^m \sum_{j=1}^n \mathcal{K}(\mathbf{x}_i, \mathbf{y}_j), \end{aligned} \quad (14)$$

where  $\mathcal{K}(\cdot, \cdot)$  denotes a positive-definite kernel (e.g., Gaussian RBF). By minimizing  $\text{MMD}^2(P, Q)$  over multiple source domains  $\mathcal{D}_k$ , one can align their feature distributions, potentially improving generalization to unseen domains.

#### B. Central Moment Discrepancy (CMD)

CMD aligns higher-order central moments across domains. Let  $\{\mathbf{x}_i\}_{i=1}^m$  and  $\{\mathbf{y}_j\}_{j=1}^n$  be features from two domains, each centered by subtracting its mean. Define  $\tilde{\mathbf{x}}_i$  and  $\tilde{\mathbf{y}}_j$  as the centered (and optionally normalized) features. CMD up to order  $L$  is:

$$\text{CMD}(\{\tilde{\mathbf{x}}_i\}, \{\tilde{\mathbf{y}}_j\}) = \sum_{\ell=1}^L \left\| \frac{1}{m} \sum_{i=1}^m (\tilde{\mathbf{x}}_i)^\ell - \frac{1}{n} \sum_{j=1}^n (\tilde{\mathbf{y}}_j)^\ell \right\|_2, \quad (15)$$

where  $(\tilde{\mathbf{x}}_i)^\ell$  denotes the elementwise  $\ell$ -th power of  $\tilde{\mathbf{x}}_i$ . By penalizing discrepancies in multiple moment orders, CMD encourages closer alignment between domain distributions, even when they differ in higher-order statistics.

#### C. Sliced Wasserstein Distance (SWD)

SWD approximates the high-dimensional Wasserstein distance by projecting features onto random one-dimensional subspaces. Let  $\{\mathbf{x}_i\}_{i=1}^m \in \mathbb{R}^d$  and  $\{\mathbf{y}_j\}_{j=1}^n \in \mathbb{R}^d$ , and sample a direction  $\boldsymbol{\theta}$  uniformly from the unit sphere  $\mathbb{S}^{d-1}$ . The one-dimensional Wasserstein distance (often  $W_1$ ) between the sorted projections is:

$$W_1(\boldsymbol{\theta}^\top \mathbf{x}, \boldsymbol{\theta}^\top \mathbf{y}) = \frac{1}{m} \sum_{i=1}^m \left| \hat{\mathbf{x}}_i^\theta - \hat{\mathbf{y}}_i^\theta \right|, \quad (16)$$

where  $\hat{\mathbf{x}}_i^\theta$  and  $\hat{\mathbf{y}}_i^\theta$  are the  $i$ -th smallest entries of  $\boldsymbol{\theta}^\top \mathbf{x}$  and  $\boldsymbol{\theta}^\top \mathbf{y}$ , respectively. SWD then averages  $W_1$  over many random directions:

$$\text{SWD}(\mathbf{x}, \mathbf{y}) = \mathbb{E}_{\boldsymbol{\theta} \sim \mathcal{U}(\mathbb{S}^{d-1})} [W_1(\boldsymbol{\theta}^\top \mathbf{x}, \boldsymbol{\theta}^\top \mathbf{y})]. \quad (17)$$

By sampling a sufficient number of directions, SWD provides a computationally efficient approximation to the full Wasserstein distance in  $\mathbb{R}^d$ .

In practice, MMD, CMD, and SWD can be used individually or jointly within multi-term loss functions, depending on the application requirements and data properties. Each of these alignment strategies aims to reduce inter-domain discrepancies and enhance domain generalization.

## REFERENCES

- [1] S. Wang and G. Zhou, “A review on radio based activity recognition,” *Digital Communications and Networks*, vol. 1, no. 1, pp. 20–29, 2015.
- [2] I. Nirmal, A. Khamis, M. Hassan, W. Hu, and X. Zhu, “Deep learning for radio-based human sensing: Recent advances and future directions,” *IEEE Communications Surveys & Tutorials*, vol. 23, no. 2, pp. 995–1019, 2021.
- [3] W. Jiao, C. Zhang, W. Du, and S. Ma, “WiSDA: Subdomain adaptation human activity recognition method using Wi-Fi signals,” *IEEE Transactions on Mobile Computing*, 2024.
- [4] W. Wang, A. X. Liu, M. Shahzad, K. Ling, and S. Lu, “Device-free human activity recognition using commercial wifi devices,” *IEEE Journal on Selected Areas in Communications*, vol. 35, no. 5, pp. 1118–1131, 2017.
- [5] Z. Chen, C. Cai, T. Zheng, J. Luo, J. Xiong, and X. Wang, “RF-based human activity recognition using signal adapted convolutional neural network,” *IEEE Transactions on Mobile Computing*, vol. 22, no. 1, pp. 487–499, 2021.
- [6] R. Shahbazian and I. Trubitsyna, “Human sensing by using radio frequency signals: A survey on occupancy and activity detection,” *IEEE Access*, vol. 11, pp. 40 878–40 904, 2023.
- [7] Y. Ma, G. Zhou, and S. Wang, “WiFi sensing with channel state information: A survey,” *ACM Computing Surveys (CSUR)*, vol. 52, no. 3, pp. 1–36, 2019.
- [8] J. Liu, H. Liu, Y. Chen, Y. Wang, and C. Wang, “Wireless sensing for human activity: A survey,” *IEEE Communications Surveys & Tutorials*, vol. 22, no. 3, pp. 1629–1645, 2019.
- [9] Z. Yang, Z. Zhou, and Y. Liu, “From RSSI to CSI: Indoor localization via channel response,” *ACM Computing Surveys (CSUR)*, vol. 46, no. 2, pp. 1–32, 2013.
- [10] Z. Wang, B. Guo, Z. Yu, and X. Zhou, “Wi-Fi CSI-based behavior recognition: From signals and actions to activities,” *IEEE Communications Magazine*, vol. 56, no. 5, pp. 109–115, 2018.
- [11] X. Zhou, W. Liang, I. Kevin, K. Wang, H. Wang, L. T. Yang, and Q. Jin, “Deep-learning-enhanced human activity recognition for Internet of healthcare things,” *IEEE Internet of Things Journal*, vol. 7, no. 7, pp. 6429–6438, 2020.
- [12] J. Yang, H. Zou, and L. Xie, “SecureSense: Defending adversarial attack for secure device-free human activity recognition,” *IEEE Transactions on Mobile Computing*, vol. 23, no. 1, pp. 823–834, 2022.
- [13] I. Ahmad, A. Ullah, and W. Choi, “WiFi-based human sensing with deep learning: Recent advances, challenges, and opportunities,” *IEEE Open Journal of the Communications Society*, 2024.

- [14] F. Miao, Y. Huang, Z. Lu, T. Ohtsuki, G. Gui, and H. Sari, "Wi-Fi sensing techniques for human activity recognition: Brief survey, potential challenges, and research directions," *ACM Computing Surveys*, 2024.
- [15] Z. Chen, Q. Zhu, Y. C. Soh, and L. Zhang, "Robust human activity recognition using smartphone sensors via CT-PCA and online SVM," *IEEE Transactions on Industrial Informatics*, vol. 13, no. 6, pp. 3070–3080, 2017.
- [16] U. M. Nunes, D. R. Faria, and P. Peixoto, "A human activity recognition framework using max-min features and key poses with differential evolution random forests classifier," *Pattern Recognition Letters*, vol. 99, pp. 21–31, 2017.
- [17] Y. Zhang, X. Wang, Y. Wang, and H. Chen, "Human activity recognition across scenes and categories based on CSI," *IEEE Transactions on Mobile Computing*, 2020.
- [18] J. Zhang, F. Wu, B. Wei, Q. Zhang, H. Huang, S. W. Shah, and J. Cheng, "Data augmentation and dense-LSTM for human activity recognition using WiFi signal," *IEEE Internet of Things Journal*, vol. 8, no. 6, pp. 4628–4641, 2020.
- [19] B. Li, W. Cui, W. Wang, L. Zhang, Z. Chen, and M. Wu, "Two-stream convolution augmented transformer for human activity recognition," in *Proceedings of the AAAI Conference on Artificial Intelligence*, vol. 35, no. 1, 2021, pp. 286–293.
- [20] S. Li, T. Zhu, F. Duan, L. Chen, H. Ning, C. Nugent, and Y. Wan, "HARMamba: Efficient and lightweight wearable sensor human activity recognition based on bidirectional Mamba," *IEEE Internet of Things Journal*, 2024.
- [21] D. Wang, J. Yang, W. Cui, L. Xie, and S. Sun, "Airfi: empowering wifi-based passive human gesture recognition to unseen environment via domain generalization," *IEEE Transactions on Mobile Computing*, vol. 23, no. 2, pp. 1156–1168, 2022.
- [22] J. Liu, Y. Huang, X. Shi, X. Ren, T. Mi, and R. C. Qiu, "TF-Mamba: A lightweight state space model for Wi-Fi-based human activity recognition," *IEEE Sensors Journal*, 2024.
- [23] Y. Chang, A. Mathur, A. Isopoussu, J. Song, and F. Kawsar, "A systematic study of unsupervised domain adaptation for robust human-activity recognition," *Proceedings of the ACM on Interactive, Mobile, Wearable and Ubiquitous Technologies*, vol. 4, no. 1, pp. 1–30, 2020.
- [24] E. Soleimani and E. Nazerfard, "Cross-subject transfer learning in human activity recognition systems using generative adversarial networks," *Neurocomputing*, vol. 426, pp. 26–34, 2021.
- [25] J. Yang, Y. Xu, H. Cao, H. Zou, and L. Xie, "Deep learning and transfer learning for device-free human activity recognition: A survey," *Journal of Automation and Intelligence*, vol. 1, no. 1, p. 100007, 2022.
- [26] Y. Tang, X. Liu, X. Yu, D. Zhang, J. Lu, and J. Zhou, "Learning from temporal spatial cubism for cross-dataset skeleton-based action recognition," *ACM Transactions on Multimedia Computing, Communications, and Applications (TOMM)*, vol. 18, no. 2, pp. 1–24, 2022.
- [27] Y. Ganin, E. Ustinova, H. Ajakan, P. Germain, H. Larochelle, F. Laviolette, M. March, and V. Lempitsky, "Domain-adversarial training of neural networks," *Journal of Machine Learning Research*, vol. 17, no. 59, pp. 1–35, 2016.
- [28] M. Long, Y. Cao, J. Wang, and M. Jordan, "Learning transferable features with deep adaptation networks," in *International Conference on Machine Learning*. PMLR, 2015, pp. 97–105.
- [29] J. Wang, C. Lan, C. Liu, Y. Ouyang, T. Qin, W. Lu, Y. Chen, W. Zeng, and S. Y. Philip, "Generalizing to unseen domains: A survey on domain generalization," *IEEE Transactions on Knowledge and Data Engineering*, vol. 35, no. 8, pp. 8052–8072, 2022.
- [30] X. Qin, J. Wang, Y. Chen, W. Lu, and X. Jiang, "Domain generalization for activity recognition via adaptive feature fusion," *ACM Transactions on Intelligent Systems and Technology*, vol. 14, no. 1, pp. 1–21, 2022.
- [31] H. Li, S. J. Pan, S. Wang, and A. C. Kot, "Domain generalization with adversarial feature learning," in *Proceedings of the IEEE Conference on Computer Vision and Pattern Recognition*, 2018, pp. 5400–5409.
- [32] K. Zhou, Z. Liu, Y. Qiao, T. Xiang, and C. C. Loy, "Domain generalization: A survey," *IEEE Transactions on Pattern Analysis and Machine Intelligence*, vol. 45, no. 4, pp. 4396–4415, 2022.
- [33] Y. Ding, L. Wang, B. Liang, S. Liang, Y. Wang, and F. Chen, "Domain generalization by learning and removing domain-specific features," *Advances in Neural Information Processing Systems*, vol. 35, pp. 24 226–24 239, 2022.
- [34] D. Tse and P. Viswanath, *Fundamentals of wireless communication*. Cambridge University Press, 2005.
- [35] A. G. Stove, "Linear fmcw radar techniques," in *IEE Proceedings F (Radar and Signal Processing)*, vol. 139, no. 5. IET, 1992, pp. 343–350.
- [36] V. C. Chen, F. Li, S.-S. Ho, and H. Wechsler, "Micro-doppler effect in radar: phenomenon, model, and simulation study," *IEEE Transactions on Aerospace and Electronic Systems*, vol. 42, no. 1, pp. 2–21, 2006.
- [37] D. Halperin, W. Hu, A. Sheth, and D. Wetherall, "Tool release: Gathering 802.11 n traces with channel state information," *ACM SIGCOMM Computer Communication RReview*, vol. 41, no. 1, pp. 53–53, 2011.
- [38] W. Taylor, S. A. Shah, K. Dashtipour, J. Le Kerrec, Q. H. Abbasi, K. Assaleh, K. Arshad, and M. A. Imran, "Wireless sensing for human activity recognition using USRP," in *EAI International Conference on Body Area Networks*. Springer, 2021, pp. 52–62.
- [39] Y. Kim and H. Ling, "Human activity classification based on micro-Doppler signatures using a support vector machine," *IEEE Transactions on Geoscience and Remote Sensing*, vol. 47, no. 5, pp. 1328–1337, 2009.
- [40] Y. Tian, J. Zhang, J. Wang, Y. Geng, and X. Wang, "Robust human activity recognition using single accelerometer via wavelet energy spectrum features and ensemble feature selection," *Systems Science & Control Engineering*, vol. 8, no. 1, pp. 83–96, 2020.
- [41] J. Ding and Y. Wang, "WiFi CSI-based human activity recognition using deep recurrent neural network," *IEEE Access*, vol. 7, pp. 174 257–174 269, 2019.
- [42] M. Thukral, H. Haresamudram, and T. Ploetz, "Cross-domain har: Few shot transfer learning for human activity recognition," *ACM Transactions on Intelligent Systems and Technology*, 2023.
- [43] Z.-K. Zhao and T. Hasegawa, "Domain-robust pre-training method for the sensor-based human activity recognition," in *2022 International Conference on Machine Learning and Cybernetics (ICMLC)*. IEEE, 2022, pp. 67–71.
- [44] Z. Zhou, Y. Zhang, X. Yu, P. Yang, X.-Y. Li, J. Zhao, and H. Zhou, "Xhar: Deep domain adaptation for human activity recognition with smart devices," in *2020 17th Annual IEEE International Conference on Sensing, Communication, and Networking (SECON)*. IEEE, 2020, pp. 1–9.
- [45] Y.-S. Chen, C.-Y. Li, and T.-Y. Juang, "Dynamic associate domain adaptation for human activity recognition using wifi signals," in *2022 IEEE Wireless Communications and Networking Conference (WCNC)*. IEEE, 2022, pp. 1809–1814.
- [46] Y. Yao, H. Zhang, Z. Bai, P. Xia, C. Liu, F. Geng, L. Du, X. Chen, Z. Li, P. Wang *et al.*, "Unobtrusive high-generalization fall detection: A domain-generalization framework," *IEEE Sensors Journal*, 2024.
- [47] J. Liu, W. Zhu, D. Li, X. Hu, and L. Song, "Domain generalization with semi-supervised learning for people-centric activity recognition," *Science China Information Sciences*, vol. 68, no. 1, p. 112103, 2025.
- [48] S. Ding, Z. Chen, T. sheng, and J. Luo, "Rf-net: A unified meta-learning framework for RF-enabled one-shot human activity recognition," in *Proceedings of the 18th Conference on Embedded Networked Sensor Systems*, 2020, pp. 517–530.
- [49] J. Zhao, F. Deng, H. He, and J. Chen, "Local domain adaptation for cross-domain activity recognition," *IEEE Transactions on Human-Machine Systems*, vol. 51, no. 1, pp. 12–21, 2020.
- [50] J. Yosinski, J. Clune, Y. Bengio, and H. Lipson, "How transferable are features in deep neural networks?" *Advances in Neural Information Processing Systems*, vol. 27, 2014.
- [51] B. Sun and K. Saenko, "Deep coral: Correlation alignment for deep domain adaptation," in *Computer Vision—ECCV 2016 Workshops: Amsterdam, The Netherlands, October 8–10 and 15–16, 2016, Proceedings, Part III 14*. Springer, 2016, pp. 443–450.
- [52] V. Vapnik, "Principles of risk minimization for learning theory," *Advances in Neural Information Processing Systems*, vol. 4, 1991.
- [53] M. Arjovsky, L. Bottou, I. Gulrajani, and D. Lopez-Paz, "Invariant risk minimization," *arXiv preprint arXiv:1907.02893*, 2019.
- [54] S. Sagawa, P. W. Koh, T. B. Hashimoto, and P. Liang, "Distributionally robust neural networks for group shifts: On the importance of regularization for worst-case generalization," *arXiv preprint arXiv:1911.08731*, 2019.
- [55] A. Gretton, K. M. Borgwardt, M. J. Rasch, B. Schölkopf, and A. Smola, "A kernel two-sample test," *The Journal of Machine Learning Research*, vol. 13, no. 1, pp. 723–773, 2012.
- [56] W. Zellinger, T. Grubinger, E. Lughofer, T. Natschläger, and S. Saminger-Platz, "Central moment discrepancy (cmd) for domain-invariant representation learning," *arXiv preprint arXiv:1702.08811*, 2017.
- [57] J. Rabin, G. Peyré, J. Delon, and M. Bernot, "Wasserstein barycenter and its application to texture mixing," in *Scale Space and Variational Methods in Computer Vision: Third International Conference, SSVN 2011, Ein-Gedi, Israel, May 29–June 2, 2011, Revised Selected Papers 3*. Springer, 2012, pp. 435–446.